Synthetic Aperture Radar Image filtering by Unbiased Risk Estimates for Singular Value Thresholding and Multi-Chromatic-Analysis

Dr. Filippo Biondi, *Member, IEEE* University of L'Aquila - Via Vetoio 1 67100 L'Aquila (ITALY)

***Abstract*—The problem of chirped synthetic aperture radar (SAR) systems is the high vulnerability of the received information to speckle noise. This study proposes a valid denoising solution for SAR images or videos formed by stacks of multi-chromatic analysis (MCA) of one single look complex (SLC) SAR image. The solution consists of, using the singular value thresholding (SVT) unbiased risk estimate (URE-SVT) for automated and optimized denoising of dynamic SAR videos.**

***Index Terms*—Synthetic Aperture Radar, Image filtering, Compressed Sensing.**

I. Introduction

THIS paper demonstrate an efficient method useful to perform dynamic Synthetic Aperture Radar (SAR) series denoising using the unbiased risk estimate singular value thresholding (URE-SVT). This new method, which theory was successfully developed in [1] and applied for reducing noise in Magnetic Resonance Imaging applications, is in this paper used to drastically reduce the noise of one SAR single image or SAR videos, permitting to distinguish small targets of interest embedded in heavy clutter. The dynamic SAR condition is procured by multi chromatic analysis (MCA). This Signal Processing technique permits the information extrapolation that can be performed in the range direction or in the azimuth direction or in both dimensions. in the case of this paper the dynamic condition is performed in the range direction. The dataset used was composed by one single look complex (SLC) Spotlight-2 (SP-2) and stripmap images observed by the COSMO-SkyMed (CSK) satellite system. The target of this work is to recover low-rank data matrix from noisy observations. The task is performed assuming that the SAR video frames are one to each other in a low-rank configuration. Results are estimated in evaluating the benefits of the filtering process considering coherent SAR processing like the estimation of digital elevation models (DEMs). The technique is also used to build-up precious sea masks. A considerable time reducing of the phase unwrapping computational stage has been also observed. Numerous filtering methods has been developed for SAR applications. Most of the techniques are based on multi-look signal processing (SP) techniques. In [2] the author predicted the occurrence of speckle noise for coherent SAR image processing. The most well-known SAR image speckle filters are adaptive and based on local statistics such as mean and standard deviation. Filtering schemes based on fixed size average windows. This approach calls to trade-off between the extent of speckle noise suppression and the radar resolution loss. In [3] the author performed a detailed characterization of the SAR speckle noise, having a multiplicative nature. The work motivated the usage of adapted sigma filters to recover speckle corrupted SAR images. The algorithm based its concepts in averaging the considered pixel with other neighboring having they energy level within two noise standard deviations. Results furnished suppression of speckle with little blurring edges and resolution loss. In [4] the author described a method to predict the wavenumber dependence of the speckle component in spectra of SAR intensity images. The application was intensively used for recovering SAR spectral images observed from oceans. The method uses correlation function of the corresponding SLC SAR images. In [5] The author detailed new physical approach considering ships as dominant scatterers and, therefore, responsible for a strong and coherent backscattered signal. Ship detection bases its rationale, a new simple and very effective filtering technique, based on adaptive windowing. In [6] the author presents a phase-unwrapping (PU) algorithm for SAR interferometry that makes use of a particle filter that simultaneously performs noise filtering and PU. Full polarimetric radars requires high level speckle filter requirements. In [7] a new filtering technique for the interferometric synthetic aperture radar (InSAR) phase has been presented. The algorithm use a patch based locally optimal Wiener filter using both geometrical and radiometric similarities by clustering analysis and nonlocal filtering. In [8] an effective the sigma filter improvement algorithm for the SAR polarimetric case is presented. The algorithm propose the scattering mechanism preservation in addition to speckle noise reduction. In [9] the authors described a new concept in polarimetric SAR speckle filtering that preserves the dominant scattering mechanism of each image pixel. The algorithm first applies the Freeman and Durden decomposition to separate pixels into the three polarimetric dominant scatterers categories and then unsupervised classification is applied. Speckle filtering is performed using the classification result map as a mask. The Lee sigma filter, developed in 1983 is based on two sigma-probability. This algorithm was reasonably effective in speckle filtering. However, deficiencies were discovered in producing biased estimation and in blurring and depressing strong reflected targets. In [10] an extension of the Lee sigma filter is proposed by reducing these problems. The bias problem is solved redefining the sigma range based on the speckle probability density functions. To mitigate the problems of blurring and depressing strong reflective scatterers, a target signature preservation technique is developed. In this paper

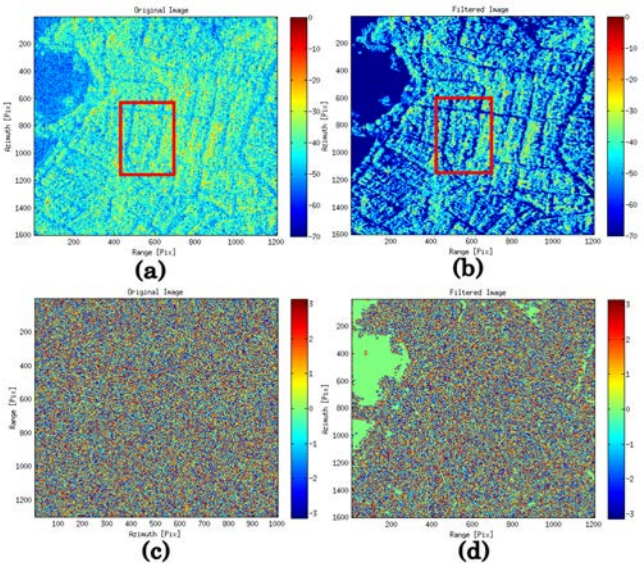

Fig. 1. Satellite images. (a): Original (Span). (b): Filtered (Span). (c): Original (Phase). (d): Filtered (Phase).

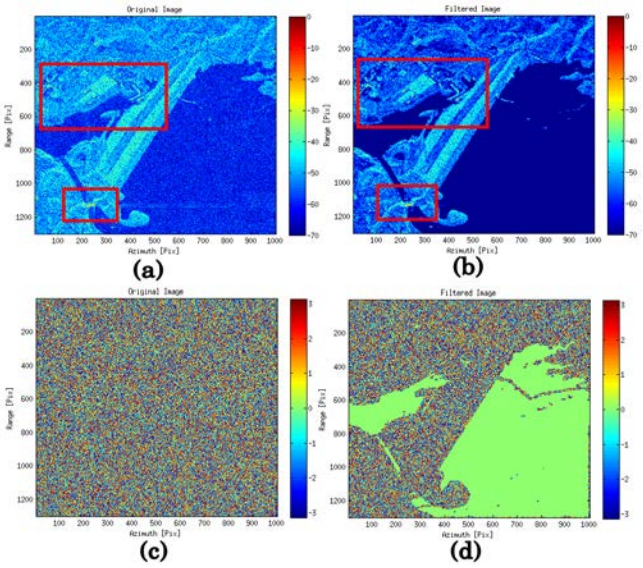

Fig. 2. Satellite images. (a): Original (Span). (b): Filtered (Span). (c): Original (Phase). (d): Filtered (Phase).

base the methodology of SAR speckle reduction recovering approximately low-rank data matrix from noisy observations. The paper demonstrate the potential use of SVT unbiased risk estimate for automated and optimized noising reduction of SAR images. The task is to denoise or the single SAR image or the same image streamed in multiple chirp or Doppler sub-apertures. The algorithm to be effective, use a stack of 200 SAR images, refocused from one single RAW image. The multi chromatic analysis (MCA) of SAR images is able to transform one image in a video, where targets can be observed in different chromatic views when captured in their chirp or Doppler domain. The MCA approach is successfully applied in [11] for generating multiple Doppler sub-aperture images of a single full-band SAR acquisition. The comparison of results showed that the method based on SVT unbiased risk estimate performed better than the state-of-the-art techniques. The author remarks the fact that the input request of the proposed algorithm is one SAR RAW image.

II. Methodology

SAR images can be considered by the sum of a low-rank component plus a sparse component. Supposing to have noise observations $\mathbf{Y}$ constituted by an SLC SAR image having $n \times m$ range-azimuth resolution cells, where the observations are referred to the synthetic data $\mathbf{X_0}$. Users are interested to recover a noiseless observation version of $\mathbf{Y}$. The above mentioned theory can be formally described by the following model:

$$Y_{i,j} = X_{0_{i,j}} + W_{i,j}, \text{ where } W_{i,j} \sim (0, \tau^2); \quad i = 1, ..., n \text{ and } j = 1, ..., m. \tag{1}$$

The optimum task of model (1) is to estimate the synthetic environment $\mathbf{X_0}$ as accurate as possible. This paper considers the condition when some structure of $\mathbf{X_0}$ can be approximated with low-rank structures. The above mentioned condition is often met since the synthetic environment $\mathbf{X_0}$ is constituted by a stack of MCA SLC sub-products estimated from a unique native SAR image. For instance the low-rank condition exists on the columns of each individual frames of the MCA video SAR sequence.

a) Singular Value Thresholding: If the object of interest has approximately low-rank, the estimate of the synthetic environment $\hat{\mathbf{X}}_\mathbf{0} = \mathbf{Y}$, can be improved in precision. The approach consists in truncating the singular value decomposition (SVD) of the observed matrix $\mathbf{Y}$, solving the following problem:

$$\text{SVHT}_\lambda(\mathbf{Y}) = \arg \min_{\mathbf{X} \in \mathbb{R}^{\mathbf{n} \times \mathbf{m}}} \frac{1}{2} ||\mathbf{X} - \mathbf{X}||_F^2 + \lambda \cdot \text{rank}(\mathbf{X}). \tag{2}$$

The parameter λ of equation (2) is a positive scalar. The SVD of the matrix $\mathbf{Y}$ is:

$$\text{SVTH}_\lambda(\mathbf{Y}) = \mathbf{U\Gamma V}^* = \sum_{i=1}^{\min(n,m)} \mathbb{I}(\sigma_i > \lambda) \mathbf{u}_i \mathbf{v}_i^*. \tag{3}$$

The SVT solution of (3) is obtained by considering only the expansion components greater than the parameter λ. The above mentioned method implies the application of a hard-thresholding on the matrix $\mathbf{Y}$ that implies several discontinuous problems on the estimate solution. This paper threats the alternative use of a soft-thresholding role to estimate the singular values. This alternative approach is described by the following model:

$$\text{SVT}_\lambda(\mathbf{Y}) = \mathbf{U\Gamma V}^* = \sum_{i=1}^{\min(n,m)} (\sigma_i > \lambda) \mathbf{u}_i \mathbf{v}_i^*. \tag{4}$$

The model (4), observed being Lipschitz continuous, is a restriction of the model (3) because considers only the singular values approaching zero bounded by the positive constant λ. The model (4) can be considered an approximated estimate of the nuclear norm $|| \cdot ||_*$. Managing a precious estimate of (4)

means finding the unique solution of:

$$\min\left[\frac{1}{2}||\mathbf{Y}-\mathbf{X}||_F^2+\lambda||\mathbf{X}||_*\right]. \quad (5)$$

b) Shrinkage optimum value, the SURE formula: The problem of URE-SVT is selecting the best shrinkage value. An excessive singular value limitation could be unusable to obtain a good filtering because only targets in high bias will be detected. An excessive shrinkage limitation will only detect high variance targets. The optimum choice of the λ parameter is to minimize the following risk mean squared error:

$$\text{MSE}(\lambda)=\mathbb{E}||\mathbf{X}_0-\text{SVT}_\lambda(\mathbf{Y})||_F^2. \quad (6)$$

The model (6) recalls the synthetic environment that is unknown. If the observations follows the model (1) it is possible to dimension the following new model named Stein's Unbiased Risk Estimate (SURE):

$$\text{SURE}(\text{SVT}_\lambda)(\mathbf{Y})=-mn\tau^2+ \quad (7)$$
$$\sum_{i+1}^{\min(n,m)}\min(\lambda^2,\sigma_i^2)+2\tau^2\text{div}(\text{SVT}_\lambda(\mathbf{Y})).$$

In (7), the sequence $[\sigma_i]_{1=1}^n$ is the singular value of $\mathbf{Y}$. The mathematical operator div$(\cdot)$ denote the divergence assumed by the non-linear mapping SVT$_\lambda$. In order to proceed in having a solution to the model (1) it is necessary to find a closed-form expression for the divergence of the estimator (6). A reliable estimate of this divergence can be the following:

$$\text{div}(\text{SVT}_\lambda(\mathbf{Y}))= \quad (8)$$
$$=\sum_{i=1}^{\min(n,m)}\left[\mathbb{I}(\sigma_i>\lambda)+|m-n|\left(1-\frac{\lambda}{\sigma_i}\right)\right]+$$
$$+2\cdot\sum_{i,j=1;i\neq j}^{\min(n,m)}\frac{\sigma_i(\sigma_i-\lambda)_+}{\sigma_i^2-\sigma_j^2}.$$

This technique has been evaluated processing SAR images observed by the CSK satellite system. The numerical experiments has been performed working with 50 sub-products after the MCA decomposition of one single h5 product. in this specific case the MCA decomposition has been performed in the range direction. In order to estimate the risk (6) of (4), the following method has been used:

$$\hat{R}_i(\lambda)=\frac{1}{50}\sum_{j=1}^{50}||\text{SVT}_\lambda(\mathbf{Y}_\mathbf{j}^{(\mathbf{i})})-\mathbf{X}_0^i||_F^2. \quad (9)$$

In (9) the parameters $\left[\mathbf{Y}_\mathbf{i}^{(\mathbf{i})}\right]_{j=1}^{50}$ are independent MCA video SAR frames, estimeted using the model (1), imposing that the synthetic parameters $\mathbf{X}^0$ are equal to $\mathbf{X}_i^0$. A more efficient method is using SURE(SVT$_\lambda$)$\mathbf{Y}$, where $\mathbf{Y}$ if estimated from the model (1).

III. Experimental Results

The results are estimated using the SP-2 and the stripmap data of the CSK satellite system. Two kinds of products has been selected, the first scenario is representing the SAR SP-2 image of the city of Sydney and the second scenario is observed with a stripmap geometry and representing the Mosul (Iraq) dam. The MCA analysis has been performed refocusing the RAW image using 200 sub-apertures. The sub-aperture band refocusing was performed in the range direction. The total chirp band of the CSK SP-2, consisting of 254 MHz has been split in 200 overlapped sub-apertures each consisting of 180 MHz. Each sub-aperture central band designed to linearly shifting from 90 MHz for the lower band SAR sub-aperture observation, up to 164 MHz for the highest band SAR sub-aperture observation. The refocusing of less band consist in accepting approximately the 30 percent of range resolution loss. The author will demonstrate that this resolution loss will be less than the resolution loss produced by conventional filtering techniques, based on adaptive filtering. The URE-SVT filtering technique is compared to the Lee-redefined (LR) state of the art filtering technique. The performance are evaluated considering the modulus and the phase of the URE-SVT filtering technique. In Fig.1 (a,b,c and d) represents a particular

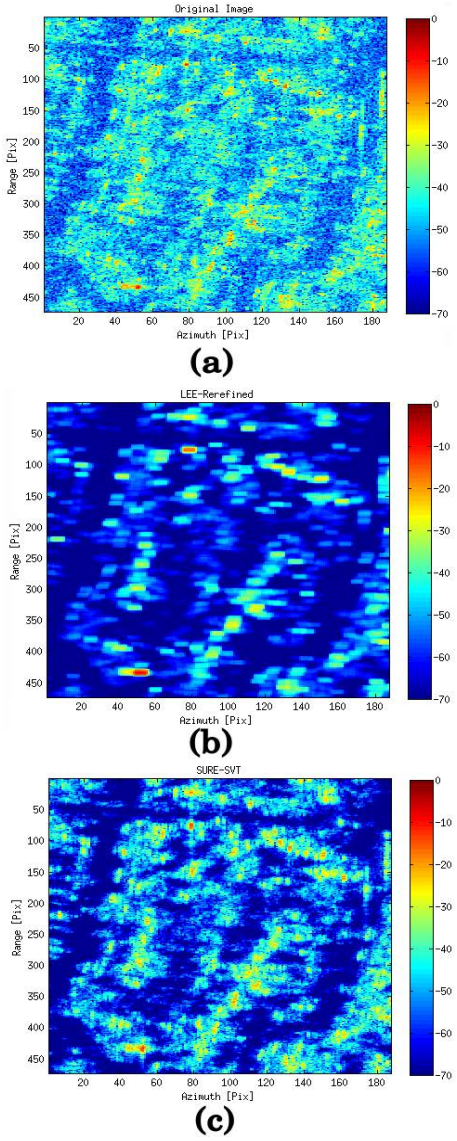

Fig. 3. Satellite images. (a): Original. (b): LR. (c): URE-SVT.

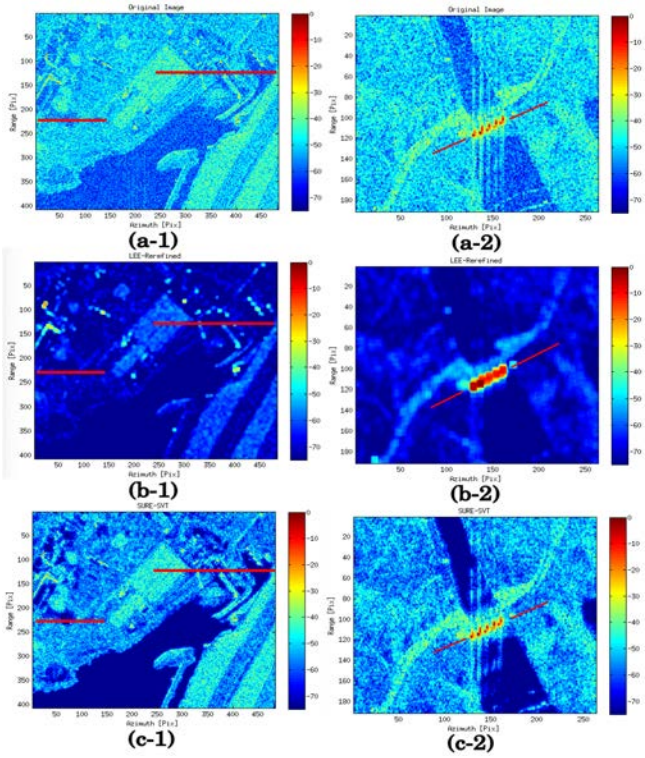

Fig. 4. Satellite images. (a): Original. (b): LR. (c): URE-SVT.

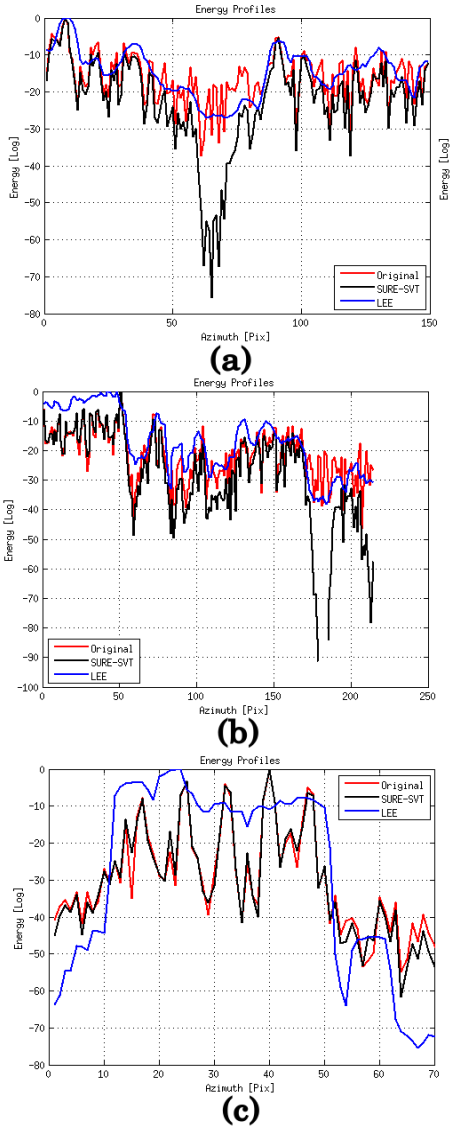

Fig. 5. Satellite images. (a): Original. (b): LR. (c): URE-SVT.

of the Sp-2 image where the substructure (a) is the energy of the original image. Fig. 1 (b,c and d) represents the URE-SVT filtering result, the phase of the original image and the phase of the URE-SVT filtered product. In Fig.2 (a,b,c and d) represents a particular of the stripmap image where the substructure (a) is the energy of the original image. Fig.2 (b,c and d) represents the URE-SVT filtering result, the phase of the original image and the phase of the URE-SVT filtered product. A high quality image filtering is observed in both the cases of study. The red boxe of Fig.1 (a and b) represents the boundaries of the images cut depicted in Fig.3 (a,b and c). Fig.3 (a) represents the original image. Fig.3 (b) is the LR filtered image and Fig.3 (c) represents the URE-SVT filtered image where a generous noise reduction with very little resolution reduction is observed. The state of the art filtering method generates a large resolution loss, visible in Fig.3 (b). In Fig.4 (a-1, a-2, b-1, b-2, c-1 and c2) the stripmap case of study results are reported, estimated from an image cut represented by the red boxes of Fig.2 (a and b). Fig. 4 (a-1 and a-2) are the original image2. Fig.4 (b-1 and b-2) are the images filtered using the LR filter and Fig.4 (c-1 and c-2) are the images filtered using the URE-SVT filter. Fig. 4 (b-1 and b-2) are the images filtered by the LR filter and Fig. 4 (c-1 and c-2) are the images processed by the URE-SVT filter. A very high-quality noise reduction without resolution loss is observed. Fig.5 (a,b and c) represents some reflectivity profiles estimated along the red lines depicted in Fig. 4 (b-1, c-1, b-1 and b-2). All the red plots are referred to the original image. The blue plots are referred to the LR filtered images and the black lines are referred to the URE-SVT filtered images. Fig.5 (a) are the energy reflectivity functions following the red line plotted on the left side to each subplots of Fig.6. The reflectivity functions of Fig.5 (b) are referred to the red line plotted on the right side to each subplots of Fig.6. Fig.5 (c) represents energy reflectivity functions estimated along the red line of Fig.7. It was noted that the URE-SVT filtering technique, works very well also on low and high SNR targets and no resolution loss is present respect to the LR filter.

IV. Conclusions

This study reported on a method useful to perform dynamic SAR series denoising using the SVT. The input of the algorithm is a single image where the dynamic SAR condition was procured by MCA performed along the range direction. results reported a very high quality filtering proprieties, also preserving the phase information where very little resolution loss has been observed.

REFERENCES

[1] E. J. Candes; C. A. Sing-Long; J. D. Trzasko. Unbiased Risk Estimates for Singular Value Thresholding and Spectral Estimators, IEEE Trans. on Signal Process. Year: 2013, Volume: 61, Issue: 19. Pages: 4643 - 4657.

[2] J.-S. Lee. A simple speckle smoothing algorithm for synthetic aperture radar images, IEEE Trans. on Systems, Man, and Cyber. Proc. IGARSS 2009, Cape Town, South Africa, July 13-17, 2009. Year: 1983, Volume: SMC-13, Issue: 1 Pages: 85 - 89.

[3] J.-M. Park; W. J. Song; W. A. Pearlman. Speckle filtering of SAR images based on adaptive windowing. IEE Proceed. - Vision, Image and Signal Process. Year: 1999, Volume: 146, Issue: 4 Pages: 191 - 197.

[4] R.A. Cordey; J.T. Macklin. Complex SAR imagery and speckle filtering for wave imaging. IEEE Trans. on Geosc. and Remote Sensing. Year: 1989, Volume: 27, Issue: 6 Pages: 665 - 673.

[5] A. Gambardella; F. Nunziata; M. Migliaccio. A Physical Full-Resolution SAR Ship Detection Filter. IEEE Geosc. and Rem Sens. Letters. Year: 2008, Volume: 5, Issue: 4. Pages: 760 - 763.

[6] J.J Martinez-Espla; T. Martinez-Marin J. M. Lopez-Sanchez. A Particle Filter Approach for InSAR Phase Filtering and Unwrapping. Year: 2009, Volume: 47, Issue: 4 Pages: 1197 - 1211.

[7] M. Mingyu Cao; S. Li; R.Wang; N, Li. Interf. Phase Denoising by Median Patch-Based Locally Optimal Wiener Filter. IEEE Geosc. and Remote Sensing Letters. Year: 2015, Volume: 12, Issue: 8. Pages: 1730 - 1734.

[8] J.-S. Lee; T.L. Ainsworth; Y. Wang; K.-S. Chen. Polarimetric SAR Speckle Filtering and the Extended Sigma Filter. IEEE Transactions on Geoscience and Remote Sensing. Year: 2015, Volume: 53, Issue: 3. Pages: 1150 - 1160, DOI: 10.1109/TGRS.2014.2335114

[9] J.-S. Lee; M. R. Grunes; D. L. Schuler; E. Pottier; L. Ferro-Famil. Scattering-model-based speckle filtering of polarimetric SAR data. IEEE Transactions on Geoscience and Remote Sensing. Year: 2006, Volume: 44, Issue: 1. Pages: 176 - 187, DOI: 10.1109/TGRS.2005.859338.

[10] J.-S. Lee; J. H. Wen; T. L. Ainsworth; K.-S. Chen; A.J. Chen. Improved Sigma Filter for Speckle Filtering of SAR Imagery IEEE Trans. on Geosc. and Remote Sensing.Year: 2009, Volume: 47, Issue: 1. Pages: 202 - 213.

[11] F. Bovenga, D. Derauw, F.M. Rana, C. Barbier, A. Refice, N. Veneziani, R. Vitulli, Multi-Chromatic Analysis of SAR images for Coherent target detection, Remote Sensing Open Access Jurnal, ISSN: 2072-4292. Doi:10.3390/rs6098822. 2014.